Experimental investigation and modeling of a reciprocating piston expander for waste heat recovery from a truck engine

Applied Thermal Engineering 186 (2021) 116425

Contents lists available at ScienceDirect

Applied Thermal Engineering

journal homepage: www.elsevier.com/locate/apthermeng

Experimental investigation and modeling of a reciprocating piston expander for waste heat recovery from a truck engine

Jelmer Rijpkema [a,*], Sandhya Thantla [b], Jens Fridh [b], Sven B. Andersson [a], Karin Munch [a]

[a] Chalmers University of Technology, Gothenburg, Sweden
[b] KTH Royal Institute of Technology, Stockholm, Sweden

ARTICLE INFO

Keywords:
Internal combustion engine
Organic Rankine cycle (ORC)
Reciprocating piston expander
Semi-empirical model
Waste heat recovery

ABSTRACT

Waste heat recovery using an (organic) Rankine cycle has the capacity to significantly increase the efficiency of heavy-duty engines and thereby reduce fuel consumption and CO_2 emissions. This paper evaluates a reciprocating piston expander used in a Rankine cycle for truck waste heat recovery by quantifying its performance on the basis of experimental results and simulations. The experimental results were obtained using a setup consisting of a 12.8 L heavy-duty Diesel engine connected to a Rankine cycle with water and are used to calibrate a semi-empirical expander model. At an engine power between 75 and 151 kW, this system recovered between 0.1 and 3 kW, resulting in an expander filling factor between 0.5 and 2.5, and a shaft isentropic effectiveness between 0.05 and 0.5. The calibrated model indicated that the heat loss (16%), mechanical loss (6–25%), pressure drop (13–42%), and leakage (25–75%) all contributed significantly to the expander performance loss. A simulation study with acetone, cyclopentane, ethanol, methanol, and R1233zd(E), showed that a change of working fluid significantly impacts the expander performance, with the filling factor varying between 0.5 and 2.2 and the effectiveness between 0.01 and 0.5, depending on the working fluid, expander speed, and pressure ratio. The results of the optimization of the built-in volume ratio and inlet valve timing during a typical long haul driving cycle showed that acetone and R1233zd(E) provided the highest available power around 3 kW absolute, or 2.2% relative to the engine. The main contributions of this paper are the presentation of experimental results of an engine coupled to a Rankine cycle, and the quantification of performance losses and the effect of working fluid variation using an adapted semi-empirical expander model, which allows for a selection of the working fluid and geometrical modifications giving optimal performance during a long haul driving cycle.

1. Introduction

The Rankine cycle (RC) is an excellent technology for waste heat recovery (WHR), enhancing the efficiency of heavy-duty engines and thereby reducing fuel consumption as well as CO_2 emissions. This is especially important considering CO_2 emissions due to road transport are increasing at a rate of about 2% per year [1]. While much effort is put into the development of electric vehicles to reduce these emissions, full electrification of heavy-duty vehicles remains challenging in the near future, making it essential to develop technologies for minimizing greenhouse gas emissions of internal combustion engines [2,3]. Other potential alternatives include currently available technologies such as dual-fuel operation, renewable fuel combustion, weight reduction, reduced resistance, and cylinder deactivation [2,4], or more advanced technologies such as hydrogen combustion, fuel cells, and free-piston engine generators [5]. Within WHR for engines, promising technologies are turbocompounding, thermo-electric generators, thermo-acoustic convertors [6,7], as well as different flash and Rankine cycles [8,9]. Of these options, the RC is an attractive candidate, with potential fuel consumption reductions of more than 5% in heavy-duty vehicles [10–12,7,13–15]. Five potential sources for waste heat can be identified within a heavy-duty engine: the charge air cooler, the engine coolant, the lubricating oil, the exhaust gas recirculation (EGR) cooler, and the exhaust gas leaving the tailpipe, where the last is mostly favored due to the relatively high temperature and mass flow [12,9,15]. To extract the heat from these sources, several architectures have been studied and implemented. The typical RC architecture consists of a single-loop, single fluid to extract the heat from only one of the available heat sources [12], occasionally with the help of an intermediate fluid such as a thermal oil [16]. Architectures utilizing multiple heat sources could use multiple fluids in a dual-loop configuration [17], or the same fluid in

* Corresponding author.
E-mail address: jelmer.rijpkema@chalmers.se (J. Rijpkema).

https://doi.org/10.1016/j.applthermaleng.2020.116425
Received 22 July 2020; Received in revised form 24 November 2020; Accepted 1 December 2020
Available online 17 December 2020

Nomenclature

A	area (m^2)
AU	global heat transfer coefficient (W/K)
c_p	specific heat capacity at constant pressure (J/kg/K)
C_d	discharge coefficient (–)
C_{loss}	frictional loss coefficient (Nm)
d	diameter (m)
f_a	supply cut-off ratio (–)
f_p	exhaust cut-off ratio (–)
h	specific enthalpy (J/kg)
L	length (m)
$\dot{m}$	mass flow rate (kg/s)
N	rotational speed (rpm)
Nu	Nussselt number (–)
P	pressure (Pa)
Pr	Prandtl number (–)
q	vapor quality (–)
$\dot{Q}$	heat transfer rate (W)
r	ratio (–)
Re	Reynolds number (–)
s	specific entropy (J/kg/K)
T	temperature (K)
U	heat transfer coefficient ($W/m^2/K$)
v	velocity (m/s)
V	volume (m^3)
$\dot{W}$	power (W)

Greek symbols

α_{loss}	proportional loss coefficient (–)
γ	heat capacity ratio (–)
$\in$	effectiveness/ error (–)
η	efficiency (–)
θ	valve timing (°)
λ	thermal conductivity (W/m/K)
μ	dynamic viscosity (Pa.s)
ρ	density (kg/m^3)
τ	torque (Nm)
ϕ	factor (–)

Subscripts

ad	adiabatic
amb	ambient
c	clearance
cp	compression
crit	critical
eff	effective
eng	engine
evc	exhaust valve closed
evo	exhaust valve open
ex	exhaust
exh	engine exhaust
exp	expander/ expansion
f	filling
int	internal
is	isentropic
iv	inlet valve
ivc	inlet valve closed
ivo	inlet valve open
leak	leakage
n	nominal
p	pressure
ref	reference
s	swept
sh	shaft
su	supply
sup	superheating
th	theoretical
thr	throat
tot	total
v	volume
w	wall

Abbreviations

ATDC	after top dead center
BDC	bottom dead center
BPV	bypass valve
EGR	exhaust gas recirculation
ESC	European stationary cycle
HW	highway
OP	operating point
ORC	organic Rankine cycle
RC	Rankine cycle
SV	safety valve
TDC	top dead center
WHR	waste heat recovery

a series [18], parallel [19,14], or cascade configuration [20], reaching up to 8% engine performance improvement. Due to the highly dynamic nature of engines, control of the WHR system is difficult and the development of dynamic models is crucial. Typically, the control objective is maximizing WHR system output power, while maintaining the vapor state at the inlet of the expander [19]. The control strategies can broadly be classified into two main classes [21]: classical control, such as PI(D) controllers [19,22,23], and advanced control, such as model predictive control [19,24]. Considering all these different aspects, the main challenge is to design and optimize the WHR system in terms of performance, costs, and packaging [25,26], while taking into account the engine operating conditions, components, cycle architectures, working fluids, and control strategies.

One of the essential components in the WHR system is the expander, which converts the recovered heat into work and thus has a crucial impact on the overall system performance. Two types of expander are commonly employed: dynamic (velocity) or volumetric (displacement). Volumetric expanders are considered more suitable for smaller WHR systems [27] because they achieve relatively high pressure ratios with low rotational speeds and flow rates, and can handle two-phase flows [28]. Of the various kinds of volumetric expanders, the most common are piston, vane, screw, and scroll expanders [27]. Among these, piston expandershave favorable characteristics for WHR in heavy-duty truck engines [29], partly because of their ability to operate at higher pressure ratios since their internal volume ratios are large [30,31]. Additionally, piston expanders typically operate at lower rotational speeds, eliminating the need to use a speed reduction gearbox for mechanical coupling to the engine [27]. Several recent experimental investigations evaluating the performance of different types of expanders for small-scale organic Rankine cycle (ORC) systems are highlighted here and summarized in Table 1. Alshammari et al. [16] investigated the performance of an ORC with a radial inflow turbine for WHR from a heavy-duty Diesel engine using an intermediate loop with thermal oil and an undisclosed working fluid. Their results showed a peak performance of 6.3 kW at an engine power of 81 kW with a pressure ratio of 5.9 and an expander speed of 15,000 rpm. A CFD model of the turbine was

developed and simulated in ANSYS CFX, of which the results showed good agreement with the experiments. In another study with a radial inflow turbine, Kaczmarczyk et al. [32] performed an experimental evaluation of an ORC in a small-scale combined heat and power system with HFE-7100 as the working fluid. The maximum generated power was 2.1 kW at a pressure ratio of 5.2 and an expander speed of 22,440 rpm. Wronski et al. [33] presented a novel reciprocating expander concept for ORC applications with a rotating variable timing admission valve system, which enabled the adjustment of the expansion ratio in real-time. The system used n-pentane and showed a maximum performance of 2.4 kW at a pressure ratio of 16.5 and an expander speed of 900 rpm. Additionally, a dynamic model was developed in Modelica, which predicted expander efficiencies within 10% and expander work within 30%. Guillaume and Lemort [25] focused on the recovery of waste heat from the exhaust gas and EGR of a heavy-duty truck with experimental results for five positive displacement expanders: piston, roots, scroll, screw and vane. All expanders used R245fa as the working fluid, except for the vane expander, where MM was used. The maximum power output varied between 1.1 and 4.7 kW for pressure ratios ranging from 1 to 11 and expander speeds from 1000 to 12,400. The experimental values were used to calibrate semi-empirical models so that the different expanders could be compared in terms of efficiency and filling factor. Bianchi et al. [34] experimentally studied the performance of a radial piston expander prototype in a micro-scale ORC system with R134a. The maximum power output was 1.2 kW at pressure ratio of 2.8 and an expander speed of 800 rpm. Campana et al. [35] converted a SANDEN scroll compressor into an expander and experimentally assessed its performance using R245fa as the working fluid. The peak power produced was 0.65 kW at a pressure ratio of around 2.2 and an expander speed of 1200 rpm. Similarly, Ziviani et al. [36] experimentally evaluated an open-drive oil-free scroll expander with R245fa as the working fluid. Its maximum power output was 3.75 kW at a pressure ratio of 5.9 and an expander speed of 2500 rpm. A semi-empirical model and an artificial neural network model were calibrated based on the experimental data and compared. Fatigati et al. [37] did an experimental comparison between a single and dual-intake sliding rotary vane expander installed on an ORC system coupled to a 3 L supercharged Diesel engine. With R236fa as the working fluid the dual-intake showed the best performance of 0.40 kW at a pressure ratio of 2 and expander speed of 1521 rpm. Their GT-Suite model showed good agreement with the experiments. Zhao et al. [38] investigated the performance of an ORC using their self-developed single screw expander for seasonal variations in the cooling water flow. Their system with R123 showed a maximum performance of 6.6 kW at pressure ratio of 6.4 and an expander speed of 3000 rpm.

Table 1
Selection of experimental results of expander performance in small-scale ORC systems.

Reference	Type (s)	Fluid(s)	r_p	N_{exp}	$\dot{W}_{exp}$	η_{exp}
–	–	–	–	rpm	kW	–
Alshammari et al. [16]	Turbine	n/a	1.4 – 5.9	5000 – 20,000	0.5 – 6.3[a]	0.10 – 0.35
Bianchi et al. [34]	Piston	R134a	1.6 – 2.7	320 – 1100	0.3 – 1.2[a]	0.38 – 0.42
Campana et al. [35]	Scroll	R245fa	1.1 – 2.7	400 – 1400	0.1 – 0.7[b]	0.10 – 0.45
Fatigati et al. [37]	Vane	R236fa	1.7 – 2.0	1520	0.3 – 0.4[b]	0.53 – 0.62
Guillaume and Lemort [25]	Piston	R245fa	6.1 – 11	1000 – 4000	0.4 – 2.0[a]	0.34 – 0.54
	Roots	R245fa	1.1 – 4.5	1050 – 11,000	0.0 – 3.1[a]	0.00 – 0.50
	Screw	R245fa	2.0 – 7.0	1000 – 12,400	0.1 – 4.7[a]	0.10 – 0.67
	Scroll	R245fa	2.5 – 6.0	2000 – 3500	0.2 – 2.0[a]	0.30 – 0.75
	Vane	MM	2.5 – 9.0	2550 – 4000	0.5 – 1.1[a]	0.40 – 0.58
Kaczmarczyk et al. [32]	Turbine	HFE-7100	4.4 – 5.5	7000 – 22,440	0.2 – 2.1[a]	0.38 – 0.71
Wronski et al. [33]	Piston	n-Pentane	10 – 16	870 – 1080	0.8 – 2.4[b]	0.53 – 0.74
Zhao et al. [38]	Screw	R123	4.1 – 6.4	3000	1.7 – 6.6[b]	0.39 – 0.43
Ziviani et al. [36]	Scroll	R245fa	3.5 – 7.5	800 – 3000	0.2 – 3.8[b]	0.12 – 0.58

[a] Electrical
[b] shaft

Another important criterion for the design is the selection of the working fluid. Bao and Zhao [29] reviewed a selection of fluids and expanders to identify an optimal combination for an effective organic Rankine cycle (ORC) system. In addition to the thermodynamic properties of the fluid, its safety and impact on the environment must be considered [13]. Water or water-based mixtures are more advantageous than organic fluids in terms of cost, thermal stability, safety, and system complexity while it has several disadvantages such as a high freezing point, high boiling temperature, and high heat of vaporization. For WHR in automotive applications, water is considered unsuitable when using turbines, as the transient conditions make it difficult to ensure dry expansion, thereby running the risk of blade erosion. The use of volumetric expanders, which are more tolerant of wet conditions during expansion, relaxes this constraint. Thus, water is considered to be one of the safest options with a few advantages for recovering waste heat, particularly from the exhaust of a heavy-duty truck engine.

The basis of this paper is an experimental investigation for the analysis of the recovery of waste heat from the exhaust gas of a heavy-duty truck engine using the Rankine cycle. The performance of a reciprocating piston expander in the RC with water as the working fluid was evaluated experimentally and the results were used to calibrate a semi-empirical model of the expander. This model was then used to quantify and evaluate the different contributions to the performance loss of the expander. Additionally, the model was expanded to include the performance for working fluids other than water. By modifying the built-in volume ratio and inlet valve timing in the model, the optimum performance during a driving cycle was estimated for each fluid. The contribution of this paper is threefold. Firstly, it presents (not widely available) experimental results of a RC WHR system with water coupled to an internal combustion engine. Secondly, by describing the model relations and quantifying the effects of different losses and working fluids, it contributes to a better understanding of the reciprocating piston expander. And lastly, the model serves as a predictive tool for the selection of the working fluid and geometrical modifications yielding the best performance in a typical long haul driving cycle.

2. Experimental setup

The experimental setup consists of a heavy-duty engine connected to a WHR system. The engine is a 12.8 L heavy-duty turbocharged Diesel engine with EGR [9] of which the exhaust gases are the heat source for a Rankine cycle using water as the working fluid. In the WHR system, the working fluid flows from the condenser (a plate heat exchanger cooled by the available process water) to the buffer tank which is open to the atmosphere. From here, the fluidflows through a filter to the inlet of the high pressure axial piston pump. From the pump, the fluid flows to the evaporator, with the possibility to recirculate part of the flow to the buffer tank via a control valve. In the evaporator (a plate heat exchanger in contact with the hot exhaust gases from the engine) steam is generated which may either enter the expander or bypass it via a controllable bypass valve (BPV), as shown in Fig. 1. The BPV is controlled during start-up to obtain the required pressure and superheating temperature at the expander inlet. An additional safety valve (SV) is installed to prevent excessive pressures in the system. Once the conditions for pressure and superheating temperature are met, the bypass valve is closed and the expander started. The superheated steam is expanded, producing power,

and then leaves the expander at a low pressure and enters the condenser. The type of sensors used and the corresponding uncertainties are shown in Table 2.The setup was monitored and controlled using two National Instruments CompactRIO 9074 controllers, which were coupled to a Labview interface. For each measuring point, the experimental values were averaged based on three minutes of collected data.

The expander, shown in Fig. 2, is a two cylinder uniflow reciprocating piston expander previously used for waste heat recovery from the EGR cooler in a heavy-duty engine [39,6]. It operates similarly to the two-stroke combustion engine: high pressure, high temperature steam enters from the top and exits at a reduced pressure and temperature at the bottom of the cylinder. The steam is admitted through the inlet port, which is normally closed by a valve attached to a valve spring and periodically opened by a push-rod mounted to the piston head. The steam exits through the outlet port, which is uncovered when the piston travels down. Both pistons are connected to the expander crankshaft, which is coupled to an electric brake via a shaft equipped with a torque and speed sensor. The bearings between the crankshaft and the crankcase necessitate a separate oil circuit, which is depicted schematically in Fig. 1. Although only a negligible amount of oil ends up in the water, a significant amount of steam enters the crankcase. To avoid adverse effects on the lubricating properties of the oil, the water is evaporated from the oil by heating it to 140 °C, and the water is expelled via an external drain. Since the oil pump cannot handle the high temperature, the oil must then be cooled down before entering the pump.

3. Expander Modeling

The expander model is a modified version of a steady state, semi-empirical model [40], originally developed for volumetric expanders such as scroll or screw expanders [41,42], and adapted for piston expanders [43,44]. The semi-empirical model relies on thermodynamic equations with several tuning parameters that must be identified using a calibration procedure that is based on the experimental results. These parameters are included to account for deviations from ideal expander performance caused by pressure drops, leakage, heat losses, and mechanical losses. By using time-averaged parameters and properties, the dynamic and sequential operation of the expander is modeled as a steady-state operation where the physical processes occur simultaneously. The model was built using the MATLAB [45] environment connected to REFPROP [46] for the fluid properties. Fig. 3 shows the Pressure–Volume (PV) diagram of the ideal expansion process for the expander, with labels referring to locations shown in Fig. 4.

At top dead center (TDC), the inlet valve is open and the expander is at its smallest volume: the clearance volume (V_c). Because of the pressure drop over the inlet port, the pressure at the start of expansion (P_{su3}) is lower than the supply pressure (P_{su}). As the expander moves downward, high-pressure steam enters the cylinder until it reaches the volume at which inlet valve closes (V_{ivc}). Expansion starts and continues until the exhaust valve opens (V_{evo}) after which the cylinder pressure

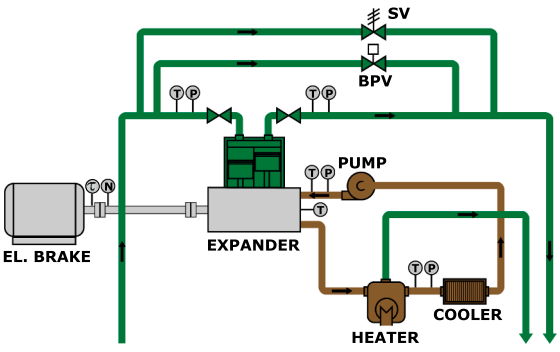

Fig. 1. Schematic depiction of the expander circuit and connecting oil circuit and electric brake.

Table 2
Measurement devices accuracy.

Input	Type	Range	Accuracy	Unit
Engine speed	Schenck D900-1e	0 – 6500	± 2	rpm
Engine torque	Schenck D900-1e	−4000 – 4000	± 8	Nm
Expander speed	HBM T40B	0 – 20000	± 10	rpm
Expander torque	HBM T40B	−500 – 500	± 0.25	Nm
Mass flow	Micro Motion F025S	0 – 100	± 0.2	g/s
Pressure	WIKA A-10	0 – 60	± 0.6	bar(g)
Temperature	RS Pro Type K	−75 – 1100	± 1.5	°C

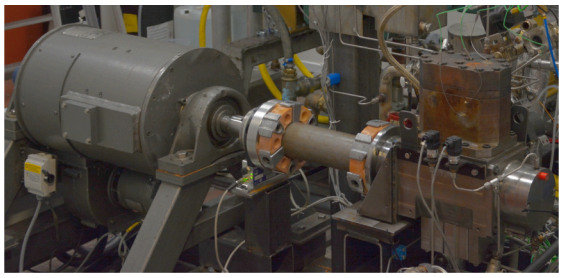

Fig. 2. The piston expander (right) connected to the torque sensor and electric brake (left).

equalizes with the exhaust pressure (P_{ex3}). The piston then travels downward at constant pressure until it reaches bottom dead center (BDC) and its maximum volume (V_{tot}). Due to the pressure drop over the outlet port, the exit pressure (P_{ex}) is lower than the expansion exhaust pressure (P_{ex3}). From here, the piston travels upward with low-pressure steam, until the exhaust valve closes (V_{evc}), which is the same volume as that at which the exhaust valve opens. The mass that is trapped when the exhaust valve closes is compressed until the inlet valve opens (V_{ivo}), at which point the pressure is equalized to the inlet pressure. With the inlet valve open, the piston will travel up until it reaches TDC, after which the cycle repeats.

3.1. Expander parameters

The measured geometrical parameters for the expander are shown in Table 3. Using these values the corresponding piston volumes can be

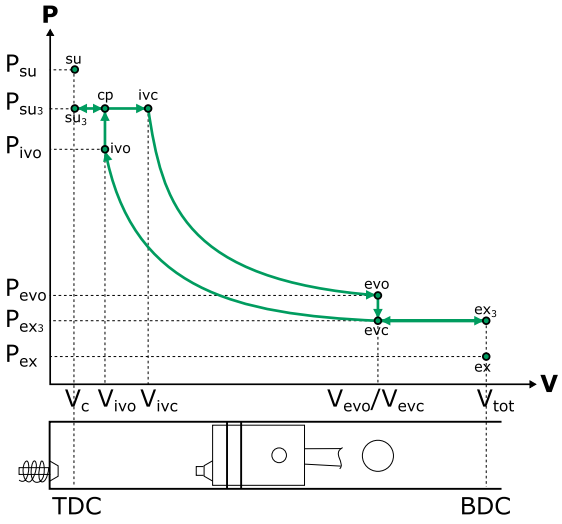

Fig. 3. Ideal PV-diagram for the operation of a uniflow reciprocating piston expander in under-expansion with a schematic representation of the corresponding piston movement in the cylinder.

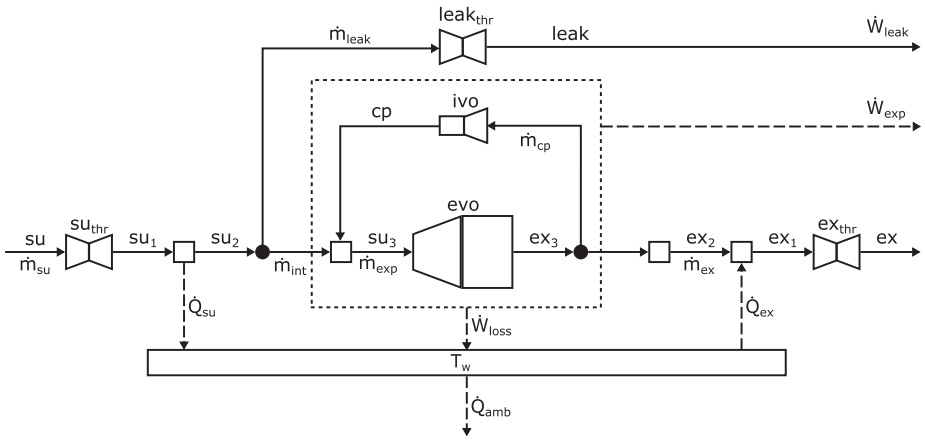

Fig. 4. The semi-empirical model piston expander model.

calculated using geometrical relations [47,6] of which the results are shown in Table 4. From these the geometrical parameters were derived: the supply and exhaust cut-off ratio (f_a and f_p), the built-in volume ratio (r_v), and the (effective) volumetric expansion and compression ratio ($r_{v,exp}$ and $r_{v,cp}$), of which the values and definitions are shown in Table 5.

The model variables were separated into three types: input variables, output variables, and tuning parameters. The input variables are equal to the experimental values and the output variables are the result of the model calculation. Both types are listed in Table 6. The tuning parameters (some of which were kept constant) are tuned during the calibration to match the output variables with the experimental values. These are listed in Table 9, together with the resulting values from the calibration.

3.2. Expander model

As mentioned, the expander model was originally developed for a scroll expander based on an existing scroll compressor model [41,42]. The model in this study, schematically depicted in Fig. 4, was modified to include the pressure drop on the exhaust side of the expansion, compression in the cylinder, leakage to the environment, and the ability to predict performance when using other working fluids. The model represents a single cylinder, so its predicted mass flows and energy changes must be multiplied by the number of cylinders in the expander when comparing its output to the experimental results.

3.2.1. Supply pressure drop ($su \rightarrow su_1$)

The adiabatic supply pressure drop is modeled by treating the supply mass flow as isentropic flow ($s_{su,thr} = s_{su}$) through a converging nozzle, shown in Eq. (1), after which the kinetic energy is converted into enthalpy ($h_{su1} = h_{su}$) at constant pressure. The supply diameter (d_{su}) represents the mean effective diameter which must be determined using the expander calibration.

$$\dot{m}_{su} = \rho_{su}\frac{\pi d_{su}^2}{4}\sqrt{2\left(h_{su} - h_{su,thr}\right)} \tag{1}$$

Table 3
Measured geometrical parameters.

Bore	B	90.0	mm
Stroke	S	60.0	mm
Clearance length	L_c	3.0	mm
Con rod length	L_{cr}	118.5	mm
Inlet valve opening	θ_{ivo}	−17	° ATDC
Inlet valve closing	θ_{ivc}	34	° ATDC
Exhaust valve opening	θ_{evo}	110	° ATDC
Exhaust valve closing	θ_{evc}	250	° ATDC

Table 4
Derived volumes.

Total volume	V_{tot}	0.4008	L
Clearance volume	V_c	0.0191	L
Swept volume	V_s	0.3817	L
Inlet valve open volume	V_{ivo}	0.0295	L
Inlet valve closed volume	V_{ivc}	0.0593	L
Exhaust valve open volume	V_{evo}	0.2969	L
Exhaust valve closed volume	V_{evc}	0.2969	L

Table 5
Derived geometrical parameters.

Supply cut-off	f_a	$= V_{ivc}/V_s$	0.16	–
Exhaust cut-off	f_p	$= V_{evc}/V_s$	0.78	–
Built-in volume ratio	r_v	$= V_{tot}/V_c$	21.0	–
Expansion ratio	$r_{v,exp}$	$= V_{evo}/V_{ivc}$	5.00	–
Compression ratio	$r_{v,cp}$	$= V_{evc}/V_{ivo}$	10.1	–

Table 6
Input and output variables.

Input		Output	
Supply temp.	T_{su}	Exhaust temp.	T_{ex}
Supply pressure	P_{su}	Expander power	$\dot{W}_{exp}$
Exhaust pressure	P_{ex}	Supply mass flow	$\dot{m}_{su}$
Expander speed	N_{exp}		
Ambient temp.	T_{amb}		

To account for supersonic flow, the throat pressure ($P_{su,thr}$) is assumed to equal the greater of the outlet pressure (P_{su1}) and the corresponding critical pressure ($P_{crit,su}$):

$$P_{su,thr} = \max\left(P_{su1}, P_{crit,su}\right) \tag{2}$$

The critical supply pressure is determined based on the relation for a perfect gas [48]:

$$P_{crit,su} = P_{su}\left(\frac{2}{\gamma_{su}+1}\right)^{\left(\frac{\gamma_{su}}{\gamma_{su}-1}\right)} \tag{3}$$

3.2.2. Supply heat transfer ($su_1 \rightarrow su_2$)

The isobaric supply heat transfer ($P_{su2} = P_{su1}$) is calculated using a fictitious envelope (representing the metal parts of the expander) with a uniform wall temperature (T_w). The relation for a single-stream steady-flow heat exchanger [49] is used to calculate the supply heat transfer, which is expressed as

$$\dot{Q}_{su} = \dot{m}_{su} c_{p,su1} \left[1 - e^{\left(\frac{-AU_{su}}{\dot{m}_{su} c_{p,su1}} \right)} \right] \left(T_{su1} - T_w \right) \tag{4}$$

The global heat transfer coefficient (AU_{su}) can be calculated with Eq. (5) by correcting the nominal global heat transfer coefficient ($AU_{su,n}$) for deviations in mass flow ($\dot{m}_{su}$) from the nominal flow ($\dot{m}_{su,n}$), derived from the relation for turbulent flow in a smooth tube [49], assuming constant fluid properties.

$$AU_{su} = AU_{su,n} \left(\frac{\dot{m}_{su}}{\dot{m}_{su,n}} \right)^{0.8} \tag{5}$$

Having determined the heat transfer, the enthalpy after heat transfer (h_{su2}) can be calculated:

$$h_{su2} = h_{su1} - \frac{\dot{Q}_{su}}{\dot{m}_{su}} \tag{6}$$

3.2.3. Leakage mass flow rate ($su_2 \rightarrow leak$)

The leakage mass flow in Eq. (7) is determined by combining the isentropic nozzle ($s_{leak,thr} = s_{su2}$) with the isobaric diffuser ($P_{leak} = P_{leak,thr}, h_{leak} = h_{su2}$), equivalent to the supply pressure drop calculation, where the average effective leakage area (A_{leak}) must be determined during the calibration.

$$\dot{m}_{leak} = \rho_{leak,thr} A_{leak} \sqrt{2 \left(h_{su2} - h_{leak,thr} \right)} \tag{7}$$

Since the leakage flow is rejected to the crankcase of the expander, rather than mixed back, the throat pressure is the greater of the ambient pressure (P_{amb}) and the critical pressure ($P_{crit,leak}$):

$$P_{leak,thr} = \max \left(P_{amb}, P_{crit,leak} \right) \tag{8}$$

$$P_{crit,leak} = P_{su2} \left(\frac{2}{\gamma_{su2} + 1} \right)^{\left(\frac{\gamma_{su2}}{\gamma_{su2} - 1} \right)} \tag{9}$$

As part of the mass flow is rejected to the environment ($\dot{m}_{leak}$), the supply flow ($\dot{m}_{su}$) is reduced to the internal flow available for expansion ($\dot{m}_{int}$), expressed as

$$\dot{m}_{int} = \dot{m}_{su} - \dot{m}_{leak} \tag{10}$$

3.2.4. Expander inlet mixing ($su_2 \rightarrow su_3$)

In the piston expander, part of the mass is compressed ($\dot{m}_{cp}$) and mixed with the internal mass at supply conditions ($\dot{m}_{int}$) at isobaric conditions ($P_{su3} = P_{su2}$), as shown in Eq. (11). The corresponding enthalpy at the start of the expansion (h_{su3}) is computed using Eq. (12).

$$\dot{m}_{exp} = \dot{m}_{int} + \dot{m}_{cp} \tag{11}$$

$$\frac{h_{su3} = \dot{m}_{int} h_{su2} + \dot{m}_{cp} h_{cp}}{\dot{m}_{exp}} \tag{12}$$

3.2.5. Expansion ($su_3 \rightarrow ex_3$)

Eq. (13) shows the total mass displaced in the expander, which is the mass available at the closing of the inlet valve ($\rho_{su3} f_a V_s$) multiplied with the rotational speed of the expander (N_{exp}).

$$\dot{m}_{exp} = \frac{N_{exp}}{60} \rho_{su3} f_a V_s \tag{13}$$

As shown in Fig. 3, the internal power during the expansion stroke ($\dot{W}_{int,exp}$) can be divided into three components: suction at constant pressure ($V_c \rightarrow V_{ivc}$), adiabatic and reversible expansion ($V_{ivc} \rightarrow V_{evo}$), and discharge at constant volume ($P_{evo} \rightarrow P_{ex3}$), resulting in the following expression:

$$\dot{W}_{int,exp} = \dot{m}_{exp} \left(h_{su3} - h_{evo} \right) + \frac{\dot{m}_{exp}}{\rho_{evo}} \left(P_{evo} - P_{ex3} \right) \tag{14}$$

The density at the end of the reversible expansion ($s_{evo} = s_{su3}$) is given by

$$\rho_{evo} = \frac{\rho_{su3}}{r_{v,exp}} \tag{15}$$

Knowing the inlet enthalpy (h_{su3}), the internal expansion power $\dot{W}_{int,exp}$), and the mass flow ($\dot{m}_{exp}$), the expander exhaust enthalpy can be calculated:

$$h_{ex3} = h_{su3} - \frac{\dot{W}_{int,exp}}{\dot{m}_{exp}} \tag{16}$$

3.2.6. Compression ($ex_3 \rightarrow cp$)

During compression, the total displaced mass over time is the mass trapped in the cylinder after the exhaust valve closes ($\rho_{ex3} f_p V_s$) multiplied by the expander speed (N_{exp}):

$$\dot{m}_{cp} = \frac{N_{exp}}{60} \rho_{ex3} f_p V_s \tag{17}$$

Analogous to the expansion, the internal power during the compression stroke can be given by

$$\dot{W}_{int,cp} = \dot{m}_{cp} \left(h_{ivo} - h_{ex3} \right) + \frac{\dot{m}_{cp}}{\rho_{ivo}} \left(P_{cp} - P_{ivo} \right) \tag{18}$$

After the reversible compression ($s_{ivo} = s_{ex3}$), the density in the cylinder will be equal to

$$\rho_{ivo} = \rho_{ex3} r_{v,cp} \tag{19}$$

When the inlet valve opens, the pressures equalize ($P_{cp} = P_{su2}$) and the resulting enthalpy is

$$h_{cp} = h_{ex3} + \frac{\dot{W}_{int,cp}}{\dot{m}_{cp}} \tag{20}$$

3.2.7. Expander exhaust mixing ($ex_3 \rightarrow ex_2$)

Since the leakage flow is rejected to the environment, no mixing occurs after the expansion exhaust, meaning constant thermodynamic properties ($P_{ex2} = P_{ex3}, h_{ex2} = h_{ex3}$) and mass flow ($\dot{m}_{ex} = \dot{m}_{int}$).

3.2.8. Exhaust heat transfer ($ex_2 \rightarrow ex_1$)

Similar to the supply heat transfer, the isobaric ($P_{ex1} = P_{ex2}$) exhaust heat transfer is calculated using the relation for a single-stream steady-flow heat exchanger [49], where the global heat transfer coefficient (AU_{ex}) is scaled by the exhaust mass flow ($\dot{m}_{ex}$), after which the enthalpy (h_{ex1}) can be calculated:

$$\dot{Q}_{ex} = \dot{m}_{ex} c_{p,ex2} \left[1 - e^{\left(\frac{-AU_{ex}}{\dot{m}_{ex} c_{p,ex2}} \right)} \right] \left(T_w - T_{ex2} \right) \tag{21}$$

$$AU_{ex} = AU_{ex,n} \left(\frac{\dot{m}_{ex}}{\dot{m}_{ex,n}} \right)^{0.8} \tag{22}$$

$$h_{ex1} = h_{ex2} + \frac{\dot{Q}_{ex}}{\dot{m}_{ex}} \tag{23}$$

3.2.9. Exhaust pressure drop ($ex_1 \rightarrow ex$)

Like the supply pressure drop, the adiabatic exhaust pressure drop combines the isentropic nozzle ($s_{ex,thr} = s_{ex1}$) with the isobaric diffuser ($h_{ex} = h_{ex1}$) to calculate the corresponding pressure downstream of the nozzle while the throat pressure is limited by the critical pressure, expressed as

$$\dot{m}_{ex} = \rho_{ex1}\frac{\pi d_{ex}^2}{4}\sqrt{2\left(h_{ex1} - h_{ex,thr}\right)} \tag{24}$$

$$P_{ex,thr} = \max\left(P_{ex}, P_{crit,ex}\right) \tag{25}$$

$$P_{crit,ex} = P_{ex1}\left(\frac{2}{\gamma_{ex1}+1}\right)^{\left(\frac{\gamma_{ex1}}{\gamma_{ex1}-1}\right)} \tag{26}$$

3.2.10. Ambient heat transfer

The ambient heat transfer depends on the global heat transfer coefficient (AU_{amb}) and the temperature difference between the fictitious wall temperature (T_w) and the ambient temperature (T_{amb}):

$$\dot{Q}_{amb} = AU_{amb}\left(T_w - T_{amb}\right) \tag{27}$$

3.2.11. Energy balance

The internal power output of the piston expander and net shaft power of the expander are given by

$$\dot{W}_{int} = \dot{W}_{int,exp} - \dot{W}_{int,cp} \tag{28}$$

$$\dot{W}_{exp} = \dot{W}_{int} - \dot{W}_{loss} \tag{29}$$

The losses in the expander are represented by three different terms:

$$\dot{W}_{loss} = \dot{W}_{loss,0} + \alpha_{loss}\dot{W}_{int} + 2\pi C_{loss}\frac{N_{exp}}{60} \tag{30}$$

To calculate the wall temperature (T_w), the energy balance containing the four different contributors to the heat transfer is solved using the following expression:

$$\dot{Q}_{su} + \dot{W}_{loss} = \dot{Q}_{ex} + \dot{Q}_{amb} \tag{31}$$

The total energy balance over the expander is then defined as:

$$\dot{m}_{su}h_{su} - \dot{m}_{ex}h_{ex} = \dot{W}_{exp} + \dot{W}_{leak} + \dot{Q}_{amb} \tag{32}$$

3.2.12. Expander performance

Typically, the expander performance is expressed using a filling factor and an isentropic efficiency. However, the definition of the filling factor (ϕ_f) for a piston expander [44], shown in Eq. (33), cannot be used since the steam expands into the two-phase region and the exhaust density (ρ_{ex}) is not known from the measured pressure and temperature. Therefore, an isentropic filling factor is introduced in Eq. (34), based on the isentropic exhaust density ($\rho_{ex,is}$), i.e. considering isentropic expansion ($s_{ex} = s_{su}$).

$$\phi_f = \frac{\dot{m}_{su}}{\dot{m}_{th}} = \frac{\dot{m}_{su}}{\frac{N_{exp}}{60}\left(\rho_{su}f_a - \rho_{ex}f_p\right)V_s} \tag{33}$$

$$\phi_{f,is} = \frac{\dot{m}_{su}}{\frac{N_{exp}}{60}\left(\rho_{su}f_a - \rho_{ex,is}f_p\right)V_s} \tag{34}$$

As the definition of the isentropic efficiency assumes adiabatic operation, it cannot be used to evaluate the expander performance [41,50]. Instead, the shaft isentropic effectiveness in Eq. (35) is used to evaluate the relative performance of the expander, based on the expander shaft power ($\dot{W}_{exp}$).

$$\epsilon_{is,sh} = \frac{\dot{W}_{exp}}{\dot{W}_{is}} = \frac{2\pi\tau_{exp}\frac{N_{exp}}{60}}{\dot{m}_{su}\left(h_{su} - h_{ex,is}\right)} \tag{35}$$

From the shaft isentropic effectiveness, the shaft power can be calculated, but the expander outlet enthalpy is still unknown. This is because the energy balance must also include the leakage power and heat loss. These terms are included in the total isentropic effectiveness ($\epsilon_{is,tot}$), defined as:

$$\begin{aligned}\epsilon_{is,tot} &= \frac{\dot{m}_{su}(h_{su} - h_{ex})}{\dot{m}_{su}\left(h_{su} - h_{ex,is}\right)} \\ &= \frac{\dot{W}_{exp} + \dot{m}_{leak}\left(h_{leak} - h_{ex}\right) + \dot{Q}_{amb}}{\dot{W}_{is}} \\ &= \epsilon_{is,sh} + \frac{\dot{W}_{leak}}{\dot{W}_{is}} + \frac{\dot{Q}_{amb}}{\dot{W}_{is}}\end{aligned} \tag{36}$$

The expander performance can also be expressed relative to the engine power:

$$\Delta\eta_{eng} = \frac{\dot{W}_{exp}}{\dot{W}_{eng}} = \frac{2\pi\tau_{exp}\frac{N_{exp}}{60}}{2\pi\tau_{eng}\frac{N_{eng}}{60}} \tag{37}$$

3.3. Change of working fluid

To evaluate expander performance for fluids other than water, the expander model can be extended using relations previously developed for scroll compressors and expanders [51,52]. In this study, A_{leak}, d_{su} and d_{ex} are considered geometrical parameters, which are not influenced by the change of fluid. Additionally, the effects of changes in lubricating properties, and thus the influence of the loss parameters ($\dot{W}_{loss,0}$, α_{loss} and C_{loss}), are ignored. Since the ambient heat transfer (AU_{amb}) is unaffected by changing the working fluid, the change of fluid only affects the thermodynamic properties and the inlet and exhaust global heat transfer coefficients (AU_{su} and AU_{ex}). The heat transfer coefficient is typically expressed as a function of the Nusselt number (Nu), thermal conductivity (λ), and a reference length (L):

$$U = \frac{\mathrm{Nu}\lambda}{L} \tag{38}$$

The relevant dimensionless numbers are defined below where the Nusselt number is defined for turbulent flow in a smooth tube [49], with $m = 0.4$ in the case of heating and $m = 0.3$ for cooling.

$$\mathrm{Nu} = 0.023\mathrm{Re}^{0.8}\mathrm{Pr}^{m} \tag{39}$$

$$\mathrm{Re} = \frac{\rho v d}{\mu} = \frac{4\dot{m}}{\pi\mu d} \tag{40}$$

$$\mathrm{Pr} = \frac{c_p\mu}{\lambda} \tag{41}$$

The new global heat transfer coefficient can now be expressed in relation to the reference coefficient:

$$\frac{AU}{AU_{ref}} = \frac{\mathrm{Nu}\lambda}{\mathrm{Nu}_{ref}\lambda_{ref}} \tag{42}$$

Filling in the dimensionless numbers and rewriting gives:

$$\frac{AU}{AU_{ref}} = \left(\frac{\mathrm{Re}}{\mathrm{Re}_{ref}}\right)^{0.8}\left(\frac{\mathrm{Pr}}{\mathrm{Pr}_{ref}}\right)^{m}\left(\frac{\lambda}{\lambda_{ref}}\right) \tag{43}$$

$$AU = AU_{\text{ref}} \left(\frac{\dot{m}}{\dot{m}_{\text{ref}}}\right)^{0.8} \left(\frac{\mu}{\mu_{\text{ref}}}\right)^{m-0.8} \left(\frac{c_{\text{p}}}{c_{\text{p,ref}}}\right)^{m} \left(\frac{\lambda}{\lambda_{\text{ref}}}\right)^{1-m} \tag{44}$$

4. Experimental results

The 12.8 L Diesel engine was operated at four engine operating points, listed in Table 7. The designations A25, A50 and B25 are taken from the European Stationary Cycle (ESC) and indicate the load percentage (25, 50, 75, 100) and speed (A, B, C) [53]. The A25 and A50 points were chosen because they account for around 70% of the total driving time during a typical long haul driving cycle [11]. Additionally, one higher speed point (B25) was added, along with a typical highway-driving point (HW).

Several quantities derived from the available measurements are presented in this section. Table 8 shows the maximum measurement error based on the rules for error propagation [54].

Themeasured expander inlet pressure and temperature are shown in Figs. 5 and 6. The mass flow and expander shaft power are shown in Figs. 7 and 8.

By controlling the pump speed and pump bypass valve position, the cycle mass flow was kept constant at each engine operating point. This was done to ensure superheated conditions at the inlet of the expander based on the available heat from the exhaust gases. As expected for a constant mass flow, the expander inlet pressure decreases for an increasing expander speed, since the displaced volume flow by the expander increases. However, the expander power output remained relatively constant, except for low pressures (<15 bar). The resulting isentropic filling factor and shaft effectiveness are shown in Figs. 9 and 10.

These results show that the filling factor is high at low expander speeds and low at high expander speeds. For the effectiveness the opposite effect is visible, with the highest effectiveness at the higher pressure ratios. Since the lower expander speeds correspond to the higher pressure ratios in the cycle, the effectiveness is the result of the relatively constant expander power over the expander speed range. The expander power can also be visualized relative to the engine power, which is shown in Fig. 11. Depending on the engine operating point, between 0.2 and 2.5% of the engine power can be recovered by this waste heat recovery system.

5. Expander calibration

The expander calibration involves tuning several parameters of the expander model so that its output matches experimental values. This was done by using the genetic algorithm available in MATLAB [45] to minimize the error function shown in Eq. (45).

$$\epsilon = \sum_{k=1}^{3} \epsilon_k = \sum_{k=1}^{3} \sqrt{\sum_{i=1}^{n} \left(\frac{x_{\text{k,mod,i}} - x_{\text{k,meas,i}}}{x_{\text{k,mod,i}}}\right)^2} \tag{45}$$

Here, $x_1 = \dot{m}_{\text{su}}, x_2 = \dot{W}_{\text{exp}}, x_3 = T_{\text{ex}}$, and n the number of experiments. The tuning parameters, of which some were kept constant, are presented in Table 9. For these parameters, the model values are compared with the experimental values in Fig. 12, which also shows lines of percentage error.

Table 7
Engine operating points.

OP	N_{eng}	τ_{eng}	$\dot{W}_{\text{eng}}$	$\dot{m}_{\text{exh}}$	T_{exh}
	rpm	Nm	kW	g/s	°C
A25	1200	600	75	180	320
HW	1200	800	101	205	345
A50	1200	1200	151	290	360
B25	1500	600	94	250	310

Table 8
Maximum measurement error for the derived quantities.

Quantity	Symbol	Max. Error
Expander shaft power	$\dot{W}_{\text{exp}}$	± 8.2%
Isentropic filling factor	$\phi_{\text{f,is}}$	± 7.2%
Isentropic shaft effectiveness	ϵ_{is}	± 8.9%
Relative expander power	$\Delta\eta_{\text{eng}}$	± 8.2%

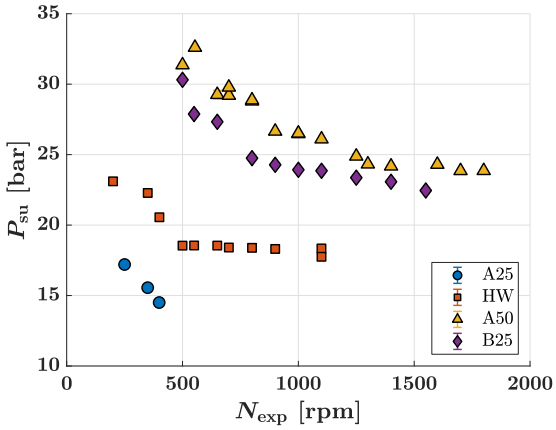

Fig. 5. The expander inlet pressure as a function of the expander speed.

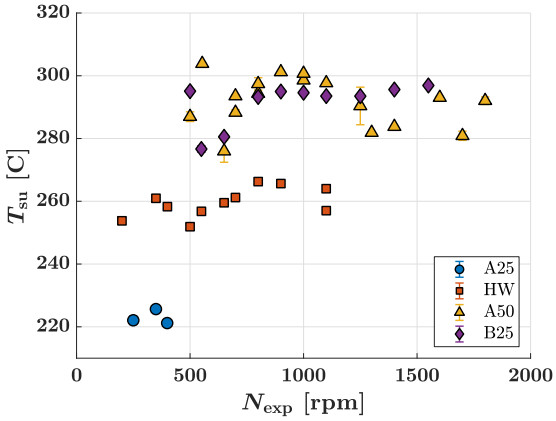

Fig. 6. The expander inlet temperature as a function of the expander speed.

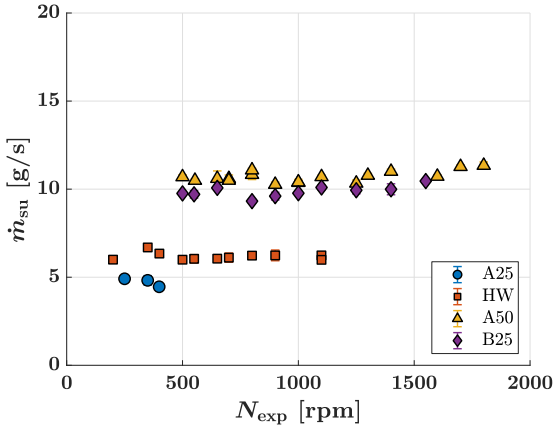

Fig. 7. The expander inlet mass flow as a function of the expander speed.

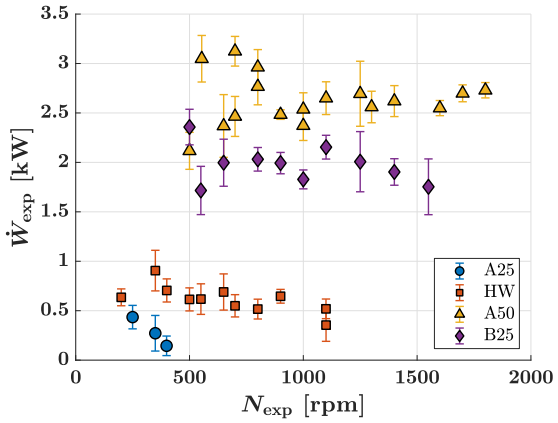

Fig. 8. The expander shaft power as a function of the expander speed.

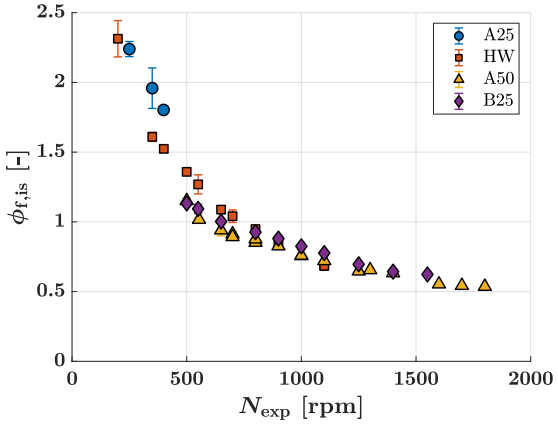

Fig. 9. The expander isentropic filling factor as a function of the expander speed.

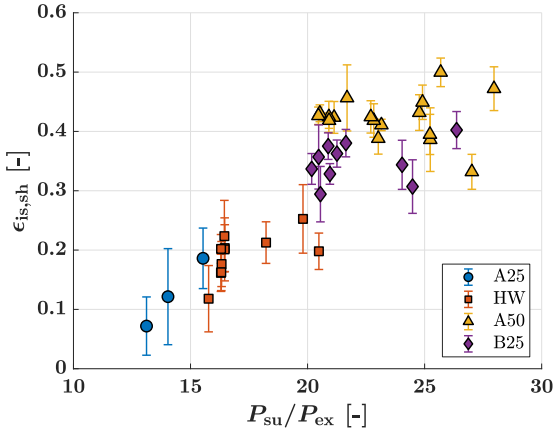

Fig. 10. The expander shaft isentropic effectiveness as a function of the pressure ratio.

Fig. 12 shows that the model is able to accurately predict the outlet temperature and predicts the mass flow reasonably well (within 10%). However, despite using the best available calibration, some model predictions of the expander power deviated significantly (by over 20%) from experiment. The model overpredicts the power at lower expander power (<1 kW) and underpredicts it at higher power (>2 kW). Possible reasons and solutions to explore in future experiments are discussed in the *Modeling Results and Discussion* section. A sensitivity analysis was

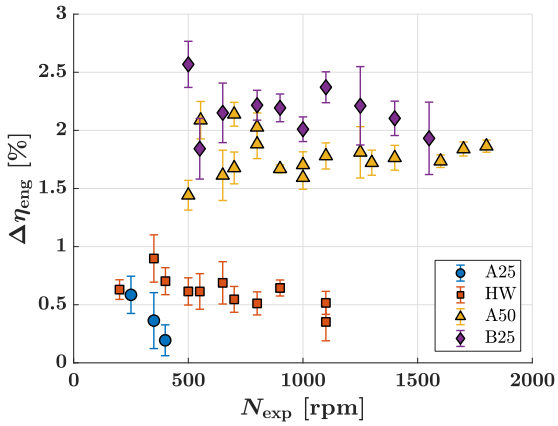

Fig. 11. The expander power relative to the engine power as a function of the expander speed.

Table 9
Fixed and calibrated tuning parameters.

Fixed			
Nominal supply mass flow	$\dot{m}_{su,n}$	0.10	kg/s
Nominal exhaust mass flow	$\dot{m}_{ex,n}$	0.10	kg/s
Calibrated			
Supply nozzle diameter	d_{su}	1.12	mm
Exhaust nozzle diameter	d_{ex}	15.6	mm
Leakage area	A_{leak}	0.648	mm^2
Supply heat transfer coef.	$AU_{su,n}$	244	W/K
Exhaust heat transfer coef.	$AU_{ex,n}$	44.7	W/K
Ambient heat transfer coef.	AU_{amb}	15.0	W/K
Constant mech. losses	$\dot{W}_{loss,0}$	106	W
Proportional mech. losses	α_{loss}	0.010	–
Frictional losses	C_{loss}	1.54	Nm

performed by varying the tuning parameters within in a range of −10% to +10%. The results are presented in Fig. 13, which shows the normalized error ($\in/\in_{min}$), where the minimum error ($\in_{min}$) is the lowest error as defined in Eq. (45). Similar to Giuffrida [55], the simulation results are most sensitive to the supply nozzle diameter (d_{su}). In comparison, the other parameters showed a negligible effect within the varied range.

6. Modeling results and discussion

The expander model helps to provide a detailed understanding of the various contributions on the performance of the expander. This section discusses the effects of these contributions on the filling factor and effectiveness as well as the effect of changing the working fluid. Subsequently, the effect of changing the built-in volume ratio and inlet valve timing for each fluid in a driving cycle is evaluated.

6.1. Expander performance

The expander performance is best expressed in terms of the filling factor (i.e. volumetric efficiency) and isentropic effectiveness (i.e. efficiency). The semi-empirical model was used to evaluate the effects of several contributions that cause deviations from the ideal performance (i.e. a filling factor and effectiveness not equal to unity), as shown in Figs. 14 and 15. The contributions were added cumulatively in the following order: *Valve clearance, Valve timing, Heat loss (internal), Heat loss (external), Mechanical loss, Pressure drop, and Leakage*. Valve clearance and valve timing represent the influence of the size of the clearance

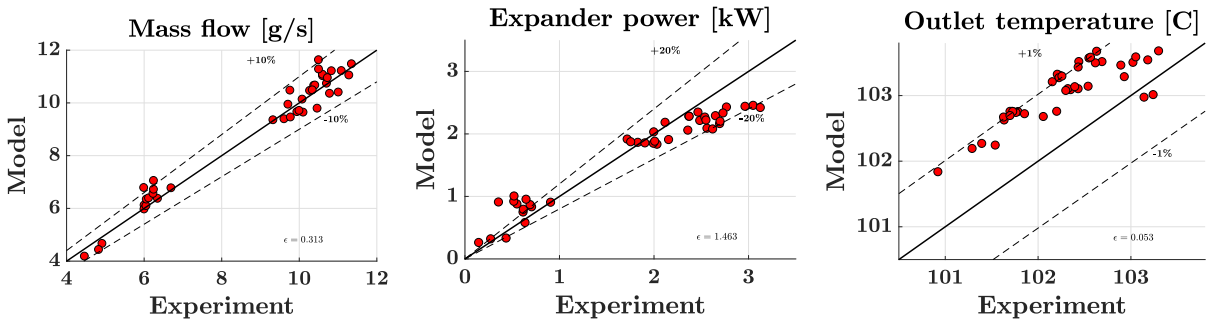

Fig. 12. Comparison of model and experimental output values after expander calibration.

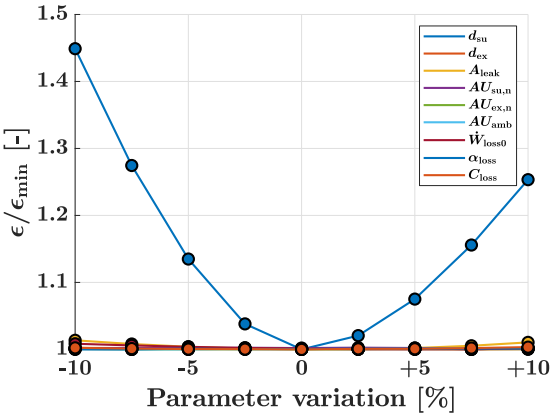

Fig. 13. Sensitivity analysis.

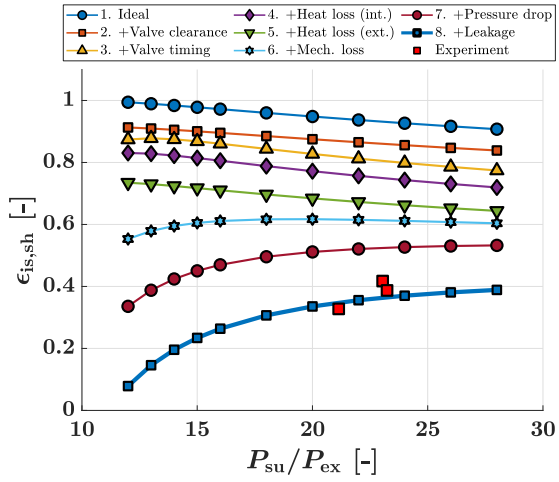

Fig. 15. Cumulative effects on the shaft isentropic effectiveness as a function of the pressure ratio with $N_{exp} = 1000$ rpm, $P_{ex} = 1.1$ bar, $\Delta T_{sup} = 60$ K.

volume (V_c) and the volumes at which the inlet and exhaust valves open and close ($V_{ivo}, V_{ivc}, V_{evo}$, and V_{evc}), respectively. Internal heat loss represents the effect of the heat transfer coefficients to the cylinder wall ($AU_{su,n}$ and $AU_{ex,n}$), but ignores the heat transfer coefficient to the ambient (AU_{amb}), which is included in the external heat loss results. Mechanical loss represents the combined effect of the different contributors to mechanical losses ($\dot{W}_{loss}, \alpha_{loss}$, and C_{loss}). Pressure drop is the effect of the supply and exhaust nozzle diameters that cause the pressure drop (d_{su} and d_{ex}), whereas the leakage results indicate the impact of the leakage area (A_{leak}).

Fig. 14 shows the cumulative effect of the contributions on the

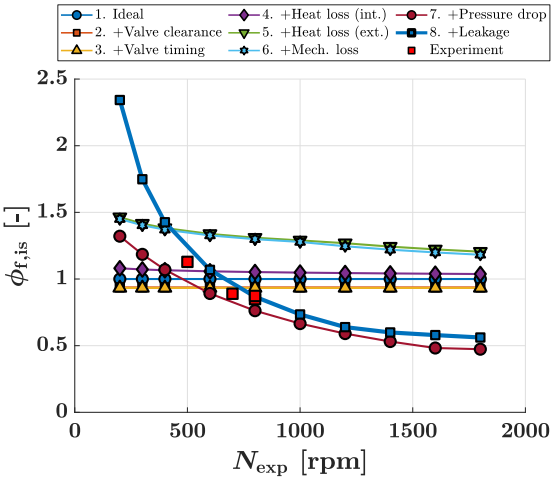

Fig. 14. Cumulative effects on the isentropic filling factor as a function of the expander speed with $P_{su}/P_{ex} = 26, P_{ex} = 1.1$ bar, $\Delta T_{sup} = 60$ K.

isentropic filling factor over a range of expander speeds. Starting at an ideal filling factor of one, the filling factor is slightly reduced by the clearance volume, but not affected by the valve timing. Both the internal and external heat loss increase the filling factor, since heat loss at the supply increases the inlet density ($\rho_{su2} > \rho_{su1}$) and heat addition to the exhaust reduces the outlet density ($\rho_{ex2} < \rho_{ex1}$). The mechanical loss has almost no effect on the filling factor, but the pressure drop reduces it significantly, especially at higher expander speeds. The pressure drop reduces the inlet density and increases the outlet density ($\rho_{su1} < \rho_{su}$ and $\rho_{ex1} > \rho_{ex}$), thereby reducing the filling factor. The effect of the leakage mass flow is highest at lower expander speeds because of the higher relative contribution of the leakage flow to the total flow. Also, the leakage mass flow decreases with increasing expander speed as a consequence of the lower supply pressure.

The corresponding shaft isentropic effectiveness is shown in Fig. 15. In the ideal case, the effectiveness reaches unity when the volumetric ratio of the fluid in the cycle matches the effective built-in volume ratio of the expander, which is determined by the valve timing ($\rho_{su3}/\rho_{ex3} = V_{ivc}/V_{evo}$). The valve clearance and valve timing cause relative performance losses of around 8 and 5%, respectively. Heat transfer reduces the performance by about 16%, with the greatest losses arising from the external heat transfer (~11%). The relative losses caused by mechanical loss, pressure drop, and leakage all decrease as the pressure ratio increases and range from 25 to 6%, 42 to 13%, and 75 to 25%, respectively. A selection of experimental and modeling results are listed in Table 10. From this selection, the small deviations between modelling and experimental results for the outlet temperatures and mass flows, and the larger deviations for the expander power, are also visible. The model allows for a prediction of the vapor quality at the outlet of the expander

(q_{ex}), which varies between 0.78 and 0.88 for all results. From the model it is also possible to identify the different contributions of the energy balance defined in Eq. (32). This shows that all contributions significantly impact the energy loss over the expander, leading to a value higher than unity for the total isentropic effectiveness, as defined in Eq. (36). These results show that all loss contributions significantly affect the expander performance. Each contribution is analyzed below to identify possible causes and improvements to reduce performance loss.

Valve clearance and Valve timing. Valve clearance and timing represent a trade-off between mechanical design and optimum performance and are determined by the expander geometry, making it difficult to modify them in the experimental setup. In a previous study [6], the valve clearance for this particular expander was increased; this resulted in similar power outputs, but shifted the optimum power to a different expander speed, allowing the expander to operate at lower inlet pressures. Another study with this expander [56], showed that the expander's power output could be doubled at available steam-delivery rates by reducing the compression ratio or extending the steam admission phase. Clemente et al. [57] reported that the supply cut-off ratio is one of the most important parameters of a reciprocating expander. Further, they note that an early cut-off results in a smaller torque but a higher ideal cycle efficiency, and vice versa. They refer to Badami and Mura [58], who concluded that the variable cut-off strategy is a good choice in terms of efficiency but presents significant challenges in technical design and construction.

Heat loss. The external heat loss represents the heat lost to the surroundings and can be reduced by insulating the expander. This will reduce the impact of the external heat loss on the effectiveness, although it will also decrease the filling factor. Insulating the expander also affects the internal heat loss because it will increase the wall temperature, thereby reducing the heat transfer at the suction and increasing it at the exhaust. A similar reduction in performance caused by heat losses was observed in another experimental study using a scroll expander [59]. In that study, the ratio of ambient losses to the electrical power from the expander ranged from 15 to 40%, despite insulation.

Mechanical loss. Mechanical losses are caused by the friction in the components of the expander, e.g. a moving piston or rotating crankshaft. The amount of friction is affected by the lubricating properties of the oil. In this setup, the crankshaft of the two cylinders of the expander was lubricated with oil from the crankcase using an oil circuit separate from the steam cycle. Due to the (significant) leakage of steam into the crankcase, the water was not fully separated from the oil, which worsened the lubricating properties of the oil over time. Reciprocating pistons are known to have large friction losses because they have many interacting surfaces, with friction between piston rings, pistons, and cylinder walls being the primary contributors. While this impact can be reduced by dissolving oil in the working fluid, lubrication difficulties may be inevitable when using reciprocating pistons with steam [29]. The use of a separate oil circuit poses an additional challenge for the implementation of this system in a truck. The extra components would require more space and the cooler would add to the cooling load of the truck. Alternatively a different separation method could be used which would not require an oil heater and cooler. Another option is the use of an expander which can be lubricated by the oil mixed directly in the working fluid.

Pressure drop. The biggest contribution to the pressure drop comes from the valves. The nozzle areas derived from the representative nozzle diameters in Eqs. (1) and (24) can also be expressed in terms of the average discharge coefficient ($\overline{C}_d$) and the average effective area ($\overline{A}_{eff}$):

$$\frac{\pi d^2}{4} = \overline{C}_d \overline{A}_{eff} \tag{46}$$

In Eq. (46) the discharge coefficient depends on the geometry and is typically expressed as a function of the Reynolds number. The effective area depends on the valve lift profile and the port area. The averages here indicate that these values represent the averaged effect during operation of valve. Again, since the valve profile and geometry depend on the expander design, modifying the experimental setup is difficult. A study on a reciprocating piston expander [43], indicated that at a constant pressure ratio, pressure losses increase with increasing rotational speed, which in turn influences the volumetric efficiency. Volumetric efficiency decreases as the expander rotational speed increases due to the rapid opening and closing of the supply valve and the associated pressure losses. Simpson et al. [60] obtained similar results in an investigation using R245fa: the maximum pressure reached at higher speeds was significantly lower than at lower speeds. Therefore, once the speed exceeds a certain limit, higher speeds reduce the mass flow rate and thus cause a reduction in volumetric efficiency, thereby reducing the effective power output. Careful valve design and timing strategies can be used to minimize these pressure losses [60].

Leakage. The pressurized steam enters the cylinders, where it leaks from the cylinders into the crankcase from where (some of) it is released into the environment. The piston contains piston rings to minimize leakage. The large amount of leakage - visible during the experiments - might indicate that the piston rings are worn out and should be replaced. The high leakage losses agree well with the results of Lemort et al. [30], who simulated a piston expander with water and a supply pressure, supply temperature, and expander rotational speed of 30 bar, 300 °C, and 3500 rpm, respectively. Their results indicated that the major losses were attributable to compression of the mass trapped inside the clearance volume and internal leakages. Also important is the lubrication of the system, especially for reciprocating pistons, since this affects the leakages via gaps between the moving seals and solid surfaces [29]. Furthermore, although leakage to the environment might be acceptable for water, it is not for the other working fluids studied in this paper.

Table 10
Comparison of a selection of experimental and modeling results.

		T_{su} °C	P_{su} bar	T_{ex} °C	P_{ex} bar	q_{ex} –	N_{exp} rpm	$\dot{m}_{su}$ g/s	$\dot{W}_{exp}$ kW	$\dot{W}_{leak}$ kW	$\dot{Q}_{amb}$ kW	$\epsilon_{is,sh}$ –	$\epsilon_{is,tot}$ –
1.	Experiment	222	17.2	102	1.1	-	250	4.9	0.44	–	–	0.19	–
	Model	222	17.2	102	1.1	0.78	250	4.7	0.33	0.96	1.75	0.15	1.37
2.	Experiment	295	30.3	103	1.1	–	500	9.8	2.36	–	–	0.40	–
	Model	295	30.3	103	1.1	0.85	500	10.5	2.06	1.35	3.38	0.33	1.08
3.	Experiment	301	26.5	102	1.1	–	1000	10.4	2.37	–	–	0.38	–
	Model	301	26.5	103	1.1	0.87	1000	10.7	2.28	0.97	3.46	0.39	1.07
4.	Experiment	292	23.8	103	1.2	–	1800	11.3	2.73	–	–	0.43	–
	Model	292	23.8	104	1.2	0.88	1800	11.5	2.34	0.76	3.56	0.36	1.02

The model predictions of the mass flow and outlet temperatures agreed quite well with the experiments (<10% and <1% respectively), as shown in Fig. 12. However, the predictions of the power were less successful, with deviations exceeding 20%. This is probably attributable to the high leakage rate, making it impossible to remove all the water from the oil while the system is running. As a result, the lubricating properties of the oil gradually worsened because of dilution with water; an effect not accounted for in the model. The high leakage rate could also directly affect the accuracy of the model. Installing new piston rings and ensuring good separation of water and oil could thus potentially improve both the expander performance and the model's agreement with experiment. Another possible source of error is the expansion in the two-phase region, visualized in Fig. 16. This shows the expander inlet and outlet conditions for point 3 of Table 10 in the Temperature-Entropy-diagram of water, together with the cumulative contributions of the energy loss over the expander as defined in Eq. (32). Since the pressure and temperature readings are not independent of one-another in the two-phase region, the thermodynamic system is not fully defined. This means that the end-state of the expansion cannot be determined from the available measurements, leading to a potential error in the fitting of the model.

6.2. Working fluids

Water was selected as the working fluid because of the availability of compatible components in the experimental setup, its reasonable thermodynamic performance, and especially its ease of handling, as it is non-toxic and non-flammable. The handling makes it an attractive working fluid, although for practical applications it is necessary to add an anti-freeze agent to lower the freezing temperature. Since water is a *wet* fluid [13], expansion ended in the two-phase region for all conditions examined in this study, possibly leading to a poor fit for the expander performance. Additionally, the definitions of the critical pressure in Eqs. (3), (9), and (26) are based on the ideal gas law, which is invalid in the two-phase region or close to the saturation line. Therefore, using a different fluid could improve the accuracy of the model, although the ideal gas law is still an approximation for heavy molecules, such as R1233zd(E). Another advantage of using an organic fluid is that the expander lubricant can be mixed into the working fluid, avoiding the need for a separate oil circuit. Replacing the working fluid in the experimental setup is not easily done, but the effect of the working fluid on the expander performance can be estimated using the calibrated model. To investigate the effect of the working fluid on the expander performance, five promising fluids [13] were simulated. To evaluate the performance of the working fluids for this particular expander, the geometry was kept constant and identical inlet conditions for the fluids were used, i.e., an outlet pressure (P_{ex}) of 1.1 bar, a superheating temperature difference (ΔT_{sup}) of 60 K, and either a pressure ratio (P_{su}/P_{ex}) of 26 or an expander speed (N_{exp}) of 1000 rpm. The results of the simulations are shown in Figs. 17 and 18. The filling factor is highest for water (2.2) and lowest for R1233zd(E) (0.9) at low expander speeds, while the value is similar for all working fluids at higher expander speeds (~0.5). There are also significant differences in effectiveness, which ranges from 0.01 to 0.13 at low pressure ratios and from 0.40 to 0.50 at higher pressure ratios. Acetone performs best over the whole range of pressure ratios.

The results in Figs. 17 and 18 are based on the definitions from the *Expander Modeling* section. The performance differences are due to the change in thermodynamic properties and heat transfer. Although it might have a significant impact, the effect of viscosity on friction is ignored. Additionally, although the nozzle diameters and leakage area from Eqs. (1), (24), and (7) are geometrical parameters, they are a function of the average effective area and discharge coefficient, as defined in Eq. (46). Whereas the area is independent of the fluid, the discharge coefficient depends on the Reynolds number. Therefore, to validate the effect on the expander performance, the same experimental setup should be used with different fluids. Two previous studies used a similar approach to model the effects of working fluids on expander performance. In one study [51], changing the fluid resulted in a difference of 200% in mass flow and a 10% change in cycle efficiency. In the other study [52], 10% differences in mass flow and expander isentropic efficiency were observed. Because of the different fluids and expanders used, it is difficult to directly compare the studies with the presented results, indicating a need for additional research.

6.3. Expander performance optimization

The calibrated model allows exploration of modifications to the original expander parameters, shown in Table 5. In this section the effect of changing the built-in volume ratio (r_v) and inlet valve timing (θ_{iv}) on the expander performance is evaluated and optimized for the different working fluids in a driving cycle. Although only simulation results are presented, some practical considerations for this expander are in order. The built-in volume ratio can be modified in two ways:

- Adding material to the top of the piston, thereby reducing the clearance volume, effectively increasing the built-in volume ratio. In the model 0.5 and 1 mm was added, leading to a built-in volume ratio of 25.0 and 31.1, respectively.
- Adding distance between the cylinder block and head, thereby increasing the clearance volume, effectively decreasing the built-in volume ratio. In the model 0.5, 1, 2, 3, and 4 mm was added, leading to a built-in volume ratio of 18.1, 16.0, 13.0, 11.0, and 9.6, respectively.

Modifying the valve timing needs more careful consideration, since changing the timing duration or the valve lift changes the valve lift profile and requires recalibration of the tuning parameters. However, the valve profile is retained if the inlet valve opening (θ_{ivo}) and closing timing (θ_{ivc}) are shifted with the same value ($\Delta\theta_{iv}$). The effect of shifting the inlet valve timing from $-10\,^\circ$ to $+10\,^\circ$ is studied in steps of $2\,^\circ$. To compare the results, the evaporator heat transfer was kept constant at each pressure ratio. A selection of the results is presented in Figs. 19 and 20, showing the effect of the built-in volume ratio and inlet valve timing on the effectiveness over a range of pressure ratios. As expected, increasing the built-in volume ratio increases the effectiveness at higher pressure ratios and decreases it at lower ratios. For the change in inlet valve timing, the effect is much less pronounced for small changes. Although, reducing the timing too much will lead to a lower performance over the whole range of pressure ratios.

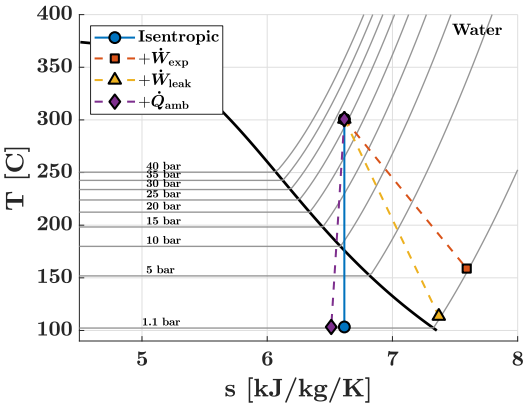

Fig. 16. Temperature-Entropy-diagram of water. Isentropic expansion of point 3 in Table 10 is shown with the cumulative effects of the expansion work ($\dot{W}_{exp}$), leakage loss ($\dot{W}_{leak}$), and heat loss ($\dot{Q}_{amb}$).

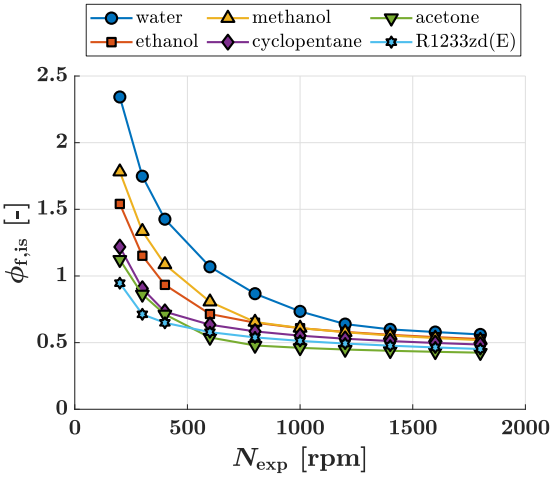

Fig. 17. The expander isentropic filling factor as a function of the expander speed with $P_{su}/P_{ex} = 26, P_{ex} = 1.1$ bar, and $\Delta T_{sup} = 60$ K.

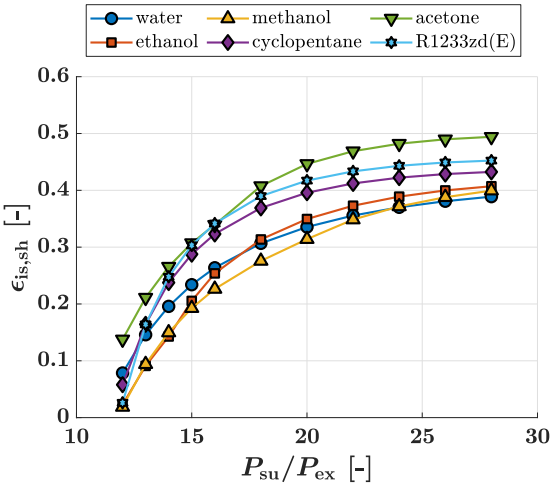

Fig. 18. The expander shaft isentropic effectiveness as a function of the pressure ratio with $N_{exp} = 1000$ rpm, $P_{ex} = 1.1$ bar and $\Delta T_{sup} = 60$ K..

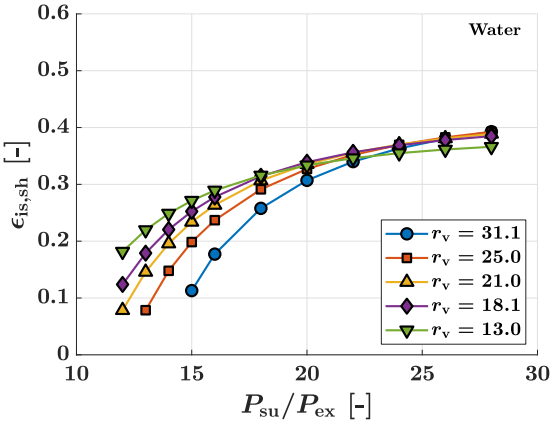

Fig. 19. Effect of the built-in volume ratio on the expander shaft isentropic effectiveness over the pressure ratio with $P_{ex} = 1.1$ bar, and $\Delta T_{sup} = 60$ K.

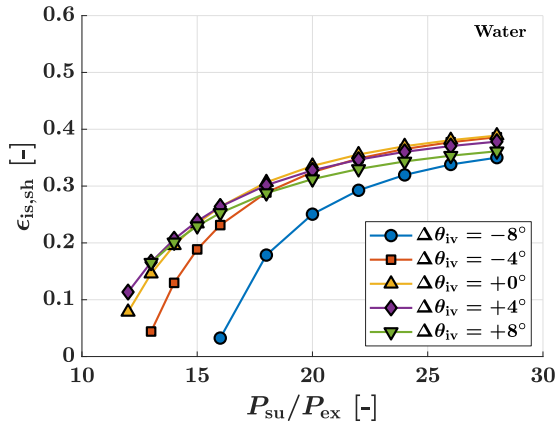

Fig. 20. Effect of the inlet valve timing on the expander shaft isentropic effectiveness over the pressure ratio with $P_{ex} = 1.1$ bar, and $\Delta T_{sup} = 60$ K.

6.3.1. *Driving cycle*

The overall performance of the system is dependent on the engine operating conditions during a driving cycle. Table 11 shows the engine operating conditions for a driving cycle with a weight (w_{dc}) based on the duration at each point for a typical long haul driving cycle [11]. Although, to be able to compare the different working fluids, a full cycle simulation is needed, the expander performance is estimated here by keeping the expander inlet pressure (P_{su}) and evaporator heat transfer ($\dot{Q}_{evap}$) constant. The values for the cycle conditions, also shown in Table 11, were taken from the experiments for A25 and A50 and extrapolated for A75 and A100 based on the experimental results. The expander inlet pressure was limited to 30 bar and the evaporator inlet temperature ($T_{evap,in}$), superheating temperature at the evaporator outlet (ΔT_{sup}), and expander outlet pressure (P_{ex}) were kept constant.

For each working fluid the expander geometry was optimized with the objective of maximizing the power output during the driving cycle. The results are presented in Table 12, which shows the built-in volume ratio (r_v) and inlet valve timing change ($\Delta\theta_{iv}$) giving the maximum power output over the driving cycle ($\dot{W}_{exp,dc}$) for each working fluid, together with the power output relative to the engine power ($\Delta\eta_{dc}$) as defined in Eq. (47). The results show that the expander power ranges from 2.0 to 3.1 kW over the driving cycle, corresponding to 1.4 to 2.2%

Table 11
Engine operating points and corresponding cycle conditions. Fixed conditions: $T_{evap,in} = 30$ °C, $\Delta T_{sup} = 60$ K, $P_{ex} = 1.1$ bar.

		Engine					Cycle	
OP	w_{dc}	N_{eng}	τ_{eng}	$\dot{W}_{eng}$	$\dot{m}_{exh}$	T_{exh}	P_{su}	$\dot{Q}_{evap}$
	-	rpm	Nm	kW	g/s	°C	bar	kW
A25	0.35	1200	600	75	180	320	17.5	6.81
A50	0.35	1200	1200	151	290	360	27.5	15.8
A75	0.20	1200	1800	226	370	395	30.0	22.9
A100	0.05	1200	2400	302	450	410	30.0	29.3

Table 12
Optimum performance of the selected working fluids over the driving cycle.

Fluid	r_v	$\Delta\theta_{iv}$	$\dot{W}_{exp,dc}$	$\Delta\eta_{dc}$
	-	°	kW	%
Acetone	25.0	0	3.1	2.2
Cyclopentane	31.1	−2	2.5	1.8
Ethanol	31.1	−2	2.0	1.4
Methanol	18.1	−2	2.3	1.7
R1233zd(E)	25.0	−2	3.0	2.2
Water	21.0	0	2.1	1.5

of power relative to the engine power. Acetone and R1233zd(E) perform best, while ethanol and water show the lowest performance for the selected fluids.

$$\Delta\eta_{dc} = \frac{\dot{W}_{exp,dc}}{\dot{W}_{eng,dc}} = \frac{\sum w_{dc,op}\dot{W}_{exp,op}}{\sum w_{dc,op}\dot{W}_{eng,op}} \quad (47)$$

7. Conclusions

A promising way to increase the efficiency of a truck engine is to use the Rankine cycle to recover heat from the exhaust gases. This paper focused on the performance of the reciprocating piston expander used in an experimental setup consisting of a 12.8 L heavy-duty Diesel engine coupled to a Rankine cycle using water as the working fluid. The experimental results were used to calibrate a semi-empirical expander model. The conclusions drawn from the experimental and modeling results are listed below.

- Four engine operating points were tested (75–151 kW) over a range of expander speeds (200–1800 rpm). Depending on the engine operating point and the expander speed, the recovered energy was between 0.1 and 3 kW in absolute terms, or between 0.1 and 2.6% relative to the engine power. The experimental results indicated that the isentropic filling factor was as high as 2.2 at low expander speeds and around 0.5 at high expander speeds. The shaft isentropic effectiveness varied between 0.05 and 0.5, mainly dependent of the pressure ratio.
- A genetic algorithm was used to calibrate parameters of the semi-empirical model based on the experimental results. The calibrated model achieved a good fit for the outlet temperature (<1%) and a reasonable fit for the mass flow (<10%), but large deviations from experiment (>20%) were observed in some cases for the expander power. The most likely causes for the lack of fit for the expander power are the high leakage flow and the expansion in the two-phase region.
- The calibrated model allows for evaluation of different contributions to the performance loss of the expander. Contributions considered in this study were valve clearance and valve timing, heat loss, mechanical loss, pressure drop, and leakage. The results showed that the filling factor increased (up to 2.2) at low expander speeds, mainly because of heat transfer and leakage. At high expander speeds it decreased (down to 0.5), primarily due to the pressure drop. The shaft isentropic effectiveness was affected significantly by all of the contributions, but especially by the mechanical loss, pressure drop and leakage. This reduced the effectiveness to less than 0.1 at low pressure ratios and to around 0.4 at higher pressure ratios. A closer look at the different contributions revealed possible causes for these reductions, and several improvements were suggested that could be tested in future simulations or experimental studies.
- To study the effect of the working fluid on expander performance, five additional fluids were simulated: acetone, cyclopentane, ethanol, methanol, and R1233zd(E). The results show that changing the working fluid significantly impacted the isentropic filling factor at low expander speeds (from 0.9 to 2.2) but had no significant impact at high expander speeds (around 0.5). Depending on the working fluid, the shaft isentropic effectiveness ranged from 0.01 to 0.13 at low pressure ratios and from 0.40 to 0.50 at high pressure ratios, with acetone offering the best performance.
- By extending the model to include geometrical modifications of the built-in volume ratio and inlet valve timing, the performance of the working fluids was optimized for a typical long haul driving cycle. This showed that the available power during the driving cycle ranged from 2.0 to 3.1 kW in absolute terms, or from 1.4 to 2.2% relative to the engine power. Acetone and R1233zd(E) offered the best performance, while ethanol and water performed worst.

Declaration of Competing Interest

The authors declare that they have no known competing financial interests or personal relationships that could have appeared to influence the work reported in this paper.

Acknowledgments

This research was made possible by funding provided by the Strategic Vehicle Research and Innovation Programme (FFI) of the Swedish Energy Agency. The authors would like to thank the partners in the WHR project: Gnutti Carlo, IAV, Lund University, Scania, TitanX, Volvo Cars, and Volvo Group.

References

[1] IEA, “CO2 Emissions from Fuel Combustion 2019: Overview,” 2019.
[2] A. García, J. Monsalve-Serrano, S. Martinez-Boggio, P. Gaillard, O. Poussin, A. A. Amer, Dual fuel combustion and hybrid electric powertrains as potential solution to achieve 2025 emissions targets in medium duty trucks sector, Energy Convers. Manage. 224 (2020).
[3] R.D. Reitz, et al., IJER editorial: The future of the internal combustion engine, Int. J. Engine Res. (2019).
[4] A. Joshi, “Review of Vehicle Engine Efficiency and Emissions,” SAE Technical Paper 2020-01-0352, 2020.
[5] A. Smallbone, B. Jia, P. Atkins, A.P. Roskilly, ”The impact of disruptive powertrain technologies on energy consumption and carbon dioxide emissions from heavy-duty vehicles,” Energy Convers. Manage.: X, vol. 6, 2020.
[6] G. Latz, Waste Heat Recovery from Combustion Engines based on the Rankine Cycle. PhD thesis, 2016.
[7] S. Lion, C.N. Michos, I. Vlaskos, C. Rouaud, R. Taccani, A review of waste heat recovery and Organic Rankine Cycles (ORC) in on-off highway vehicle Heavy Duty Diesel Engine applications, Renew. Sustain. Energy Rev. 79 (2017).
[8] S. Iglesias Garcia, R. Ferreiro Garcia, J. Carbia Carril, D. Iglesias Garcia, ”A review of thermodynamic cycles used in low temperature recovery systems over the last two years,” Renew. Sustain. Energy Rev., vol. 81, 2018.
[9] J. Rijpkema, K. Munch, S.B. Andersson, Thermodynamic potential of twelve working fluids in Rankine and flash cycles for waste heat recovery in heavy duty diesel engines, Energy 160 (2018).
[10] R. Cipollone, G. Bianchi, A. Gualtieri, D. Di Battista, M. Mauriello, F. Fatigati, Development of an Organic Rankine Cycle system for exhaust energy recovery in internal combustion engines, J. Phys: Conf. Ser. 655 (2015).
[11] S. Edwards, J. Eitel, E. Pantow, P. Geskes, R. Lutz, J. Tepas, ”Waste Heat Recovery: The Next Challenge for Commercial Vehicle Thermomanagement,” SAE Int. J. Commer. Vehic., vol. 5, no. 1, 2012.
[12] A.T. Hoang, Waste heat recovery from diesel engines based on Organic Rankine Cycle, Appl. Energy 231 (2018).
[13] J. Rijpkema, S. Andersson, K. Munch, “Thermodynamic Cycle and Working Fluid Selection for Waste Heat Recovery in a Heavy Duty Diesel Engine,” SAE Technical Paper 2018-01-1371, 2018.
[14] S. Thantla, J. Fridh, A. Erlandsson, J. Aspfors, “Performance Analysis of Volumetric Expanders in Heavy-Duty Truck Waste Heat Recovery,” SAE Technical Paper 2019-01-2266, 2019.
[15] B. Xu, D. Rathod, A. Yebi, Z. Filipi, S. Onori, M. Hoffman, A comprehensive review of organic rankine cycle waste heat recovery systems in heavy-duty diesel engine applications, Renew. Sustain. Energy Rev. 107 (2019).
[16] F. Alshammari, A. Pesyridis, A. Karvountzis-Kontakiotis, B. Franchetti, Y. Pesmazoglou, Experimental study of a small scale organic Rankine cycle waste heat recovery system for a heavy duty diesel engine with focus on the radial inflow turbine expander performance, Appl. Energy 215 (2018).
[17] E. Wang, Z. Yu, H. Zhang, F. Yang, A regenerative supercritical-subcritical dual-loop organic Rankine cycle system for energy recovery from the waste heat of internal combustion engines, Appl. Energy 190 (2017).
[18] J. Rijpkema, K. Munch, S.B. Andersson, Combining Low- and High-Temperature Heat Sources in a Heavy Duty Diesel Engine for Maximum Waste Heat Recovery Using Rankine and Flash Cycles, in: C. Junior, O. Dingel (Eds.), Energy and Thermal Management, Air-Conditioning, and Waste Heat Utilization, Springer International Publishing, 2019.
[19] E. Feru, F. Willems, B. de Jager, M. Steinbuch, ”Modeling and Control of a Parallel Waste Heat Recovery System for Euro-VI Heavy-Duty Diesel Engines,” Energies, vol. 7, no. 10, 2014.
[20] T. Chen, W. Zhuge, Y. Zhang, L. Zhang, A novel cascade organic Rankine cycle (ORC) system for waste heat recovery of truck diesel engines, Energy Convers. Manage. 138 (2017).
[21] M. Imran, R. Pili, M. Usman, F. Haglind, Dynamic modeling and control strategies of organic Rankine cycle systems: Methods and challenges, Appl. Energy 276 (2020).
[22] F. Galuppo, M. Nadri, P. Dufour, T. Reiche, V. Lemort, ”Evaluation of a Coupled Organic Rankine Cycle Mild Hybrid Architecture for Long-Haul Heavy-Duty Truck,” IFAC-PapersOnLine, vol. 52, 2019.

[23] V. Grelet, P. Dufour, M. Nadri, T. Reiche, V. Lemort, "Modeling and control of Rankine based waste heat recovery systems for heavy duty trucks," IFAC-PapersOnLine, vol. 28, 2015.
[24] H. Koppauer, W. Kemmetmüller, A. Kugi, Model predictive control of an automotive waste heat recovery system, Control Eng. Pract. 81 (2018).
[25] L. Guillaume, V. Lemort, Comparison of different ORC typologies for heavy-duty trucks by means of a thermo-economic optimization, Energy 182 (2019).
[26] M. Imran, F. Haglind, V. Lemort, A. Meroni, Optimization of organic rankine cycle power systems for waste heat recovery on heavy-duty vehicles considering the performance, cost, mass and volume of the system, Energy 180 (2019).
[27] M. Imran, M. Usman, B.-S. Park, D.-H. Lee, Volumetric expanders for low grade heat and waste heat recovery applications, Renew. Sustain. Energy Rev. (2016).
[28] O. Dumont, R. Dickes, V. Lemort, Experimental investigation of four volumetric expanders, Energy Proc. 129 (2017).
[29] J. Bao, L. Zhao, A review of working fluid and expander selections for organic Rankine cycle, Renew. Sustain. Energy Rev. 24 (2013).
[30] V. Lemort, L. Guillaume, L.A., S. Declaye, and S. Quoilin, "A comparison of piston, screw and scroll expanders for small scale Rankine cycle systems," Proceedings of the 3rd international conference on microgeneration and related technologies., 2013.
[31] H. Kanno, N. Shikazono, Experimental study on two-phase adiabatic expansion in a reciprocating expander with intake and exhaust processes, Int. J. Heat Mass Transf. 102 (2016).
[32] T.Z. Kaczmarczyk, G. Żywica, E. Ihnatowicz, Experimental study of a low-temperature micro-scale organic Rankine cycle system with the multi-stage radial-flow turbine for domestic applications, Energy Convers. Manage. 199 (2019) 111941.
[33] J. Wronski, M. Imran, M.J. Skovrup, F. Haglind, Experimental and numerical analysis of a reciprocating piston expander with variable valve timing for small-scale organic Rankine cycle power systems, Appl. Energy 247 (2019).
[34] M. Bianchi, L. Branchini, N. Casari, A. De Pascale, F. Melino, S. Ottaviano, M. Pinelli, P. Spina, A. Suman, Experimental analysis of a micro-ORC driven by piston expander for low-grade heat recovery, Appl. Therm. Eng. 148 (2019).
[35] C. Campana, L. Cioccolanti, M. Renzi, F. Caresana, Experimental analysis of a small-scale scroll expander for low-temperature waste heat recovery in Organic Rankine Cycle, Energy 187 (2019).
[36] D. Ziviani, N.A. James, F.A. Accorsi, J.E. Braun, E.A. Groll, Experimental and numerical analyses of a 5 kWe oil-free open-drive scroll expander for small-scale organic Rankine cycle (ORC) applications, Appl. Energy 230 (2018).
[37] F. Fatigati, M. Di Bartolomeo, D. Di Battista, R. Cipollone, A dual-intake-port technology as a design option for a Sliding Vane Rotary Expander of small-scale ORC-based power units, Energy Convers. Manage. 209 (2020).
[38] Y.-K. Zhao, B. Lei, Y.-T. Wu, R.-P. Zhi, W. Wang, H. Guo, C.-F. Ma, Experimental study on the net efficiency of an Organic Rankine Cycle with single screw expander in different seasons, Energy 165 (2018).
[39] G. Latz, O. Erlandsson, T. Skåre, A. Contet, S. Andersson, K. Munch, "Performance analysis of a reciprocating piston expander and a plate type exhaust gas recirculation boiler in a water-based Rankine cycle for heat recovery from a heavy duty diesel engine," Energies, vol. 9, no. 7, 2016.
[40] R. Dickes, D. Ziviani, M. de Paepe, M. van den Broek, S. Quoilin, V. Lemort, ORCmKit: an open-source library for organic Rankine cycle modelling and analysis, in: Proceedings of ECOS 2016, 2016.
[41] V. Lemort, Contribution To the Characterization of Scroll Machines in Compressor and Expander Modes. PhD thesis, 2008.
[42] V. Lemort, S. Quoilin, C. Cuevas, J. Lebrun, "Testing and modeling a scroll expander integrated into an Organic Rankine Cycle," Appl. Therm. Eng., vol. 29, no. 14–15, 2009.
[43] Y. Glavatskaya, P. Podevin, V. Lemort, O. Shonda, G. Descombes, "Reciprocating Expander for an Exhaust Heat Recovery Rankine Cycle for a Passenger Car Application," Energies, vol. 5, no. 6, 2012.
[44] J.-F. Oudkerk, Contribution to the Characterization of Piston Expanders for their Use in Small-Scale Power Production Systems. PhD thesis, 2016.
[45] MathWorks, MATLAB, Version R2019a, 2019.
[46] E.W. Lemmon, M.L. Huber, M.O. McLinden, NIST Standard Reference Database 23: Reference Fluid Thermodynamic and Transport Properties - REFPROP. National Institute of Standards and Technology, Standard Reference Data Program, Gaithersburg, 9.1 ed., 2013.
[47] J. Heywood, Internal Combustion Engine Fundamentals, McGraw-Hill, 1988.
[48] F. White, Fluid Mechanics, McGraw-Hill, 2009.
[49] A.F. Mills, Basic Heat & Mass Transfer, Prentice Hall, 1999.
[50] E. Macchi, M. Astolfi, Organic Rankine Cycle (ORC) Power Systems: Technologies and Applications, Elsevier Science, 2016.
[51] A. Giuffrida, "Modelling the performance of a scroll expander for small organic Rankine cycles when changing the working fluid," Appl. Therm. Eng., vol. 70, no. 1, 2014.
[52] M.A. Ancona, M. Bianchi, L. Branchini, A.D. Pascale, F. Melino, S. Ottaviano, A. Peretto, Performance Prediction and Design Optimization of a kW-size Reciprocating Piston Expander working with Low-GWP Fluids, in: 5th International Seminar on ORC Power Systems, 2019.
[53] "DieselNet: Emission test cycles - European Stationary Cycle (ESC)." https://www.dieselnet.com/standards/cycles/esc.php. Accessed: 2020-07-02.
[54] J. Taylor, An Introduction to Error Analysis: The Study of Uncertainties in Physical Measurements, University Science Books, 1997.
[55] A. Giuffrida, Improving the semi-empirical modelling of a single-screw expander for small organic Rankine cycles, Appl. Energy 193 (2017).
[56] G. Latz, O. Erlandsson, T. Skåre, A. Contet, "Water-based Rankine-cycle waste heat recovery systems for engines: challenges and opportunities," ASME ORC 2015, no. 2013, 2015.
[57] S. Clemente, D. Micheli, M. Reini, R. Taccani, Performance Analysis and Modeling of Different Volumetric Expanders for Small-Scale Organic Rankine Cycles, in: ASME 2011 5th International Conference on Energy Sustainability, 2011.
[58] M. Badami, M. Mura, Preliminary design and controlling strategies of a small-scale wood waste Rankine Cycle (RC) with a reciprocating steam engine (SE), Energy 34 (2009).
[59] V. Lemort, S. Declaye, S. Quoilin, Experimental characterization of a hermetic scroll expander for use in a micro-scale Rankine cycle, Proc. Inst. Mech. Eng., Part A: J. Power Energy 226 (2012) 2012.
[60] M. Simpson, G. Rotolo, P. Sapin, P. De Palma, A. White, C. Markides, "Thermodynamic performance maps of reciprocating-piston expanders for operation at off-design and part-load conditions," in: 13th International Conference on Heat Transfer, Fluid Mechanics and Thermodynamics, 2017.